Scripta Materialia 206 (2022) 114223

Contents lists available at ScienceDirect

Scripta Materialia

journal homepage: www.elsevier.com/locate/scriptamat

Surface energy contributions to the work of infiltration in metal matrix composite processing

José-Miguel Molina-Jorda[a,b], Gionata Schneider[a], Andreas Mortensen[a,*]

[a] EPFL Laboratory of Mechanical Metallurgy, Institute of Materials, Ecole Polytechnique Fédérale de Lausanne, EPFL Station 12, CH-1015 Lausanne, Switzerland

[b] Dept. of Inorganic Chemistry, University of Alicante, E-03690 San Vicente del Raspeig, Spain

ARTICLE INFO

Article history:
Received 12 July 2021
Revised 12 August 2021
Accepted 14 August 2021

Keywords:
Liquid infiltration
Capillary phenomena
Fiber reinforced composites
Metal matrix composites (MMC)
Particulate reinforced composites

ABSTRACT

The work needed to mechanically drive molten metal into a porous solid preform when producing a composite material by infiltration can significantly exceed the energy change required for thermodynamically reversible infiltration. We measure, by quantitative metallographic analysis of partially infiltrated, particle- or fiber-based non-metallic preforms, the evolution with saturation of the three interfaces present during the process. Results show that irreversible energy losses in the infiltration of alumina preforms by molten copper, aluminium or aluminium-tin alloy cannot be ascribed to the creation of liquid meniscus surface area at intermediate metal saturation. This result agrees with similar observations in soil science and gives experimental confirmation of predictions from a recent simulation of capillarity-dominated metal infiltration [*Acta Mater.*, vol. 210, 2021, 116831].

One of the principal methods used to produce composite materials is infiltration, where the matrix in fluid form is made to invade open pores within a solid "preform" of the reinforcing phase. Infiltration can produce composites with a matrix of ceramic, metal or polymer, reinforced with phases that can be chosen across a wide range of geometries, including fibres, microcellular solids, whiskers or particles [1–8].

The process of infiltration has been the subject of extensive research, both within the materials community and also in other disciplines or areas of technology, including for example soil science, reservoir engineering, CO_2 sequestration or chemical engineering. Extensive monographs and review articles exist on the subject [9–12].

From a thermodynamic standpoint, the volumetric energy required to fully and reversibly infiltrate a unit volume of porous solid preform equals the specific surface area of the reinforcement preform, S_r, times the unit area work of immersion of the solid preform, defined as:

$$W_i = \sigma_{SL} - \sigma_{SV} = -\sigma_{LV}\cos(\theta) \quad (1)$$

where σ_{SL} is the matrix/reinforcement interfacial energy, σ_{SV} is the surface energy of the dry reinforcement phase, σ_{LV} is the liquid matrix surface energy and θ is the wetting angle of the liquid matrix measured on a flat surface of the solid reinforcement phase.

In practice, the infiltration process can be highly hysteretic, meaning that expenditure of more work than $S_f W_i$ can be required to create the composite. This denotes the presence of mechanisms for irreversible energy loss as the fluid is made to invade the porous preform. Such energy loss can have several origins. The two most obvious in metal/reinforcement systems that do not form an interfacial phase by chemical reaction between the metal and the reinforcement are (i) surface energy associated with liquid/vapour interfaces that must temporarily be present within the equilibrated structure of partially saturated preforms, and (ii) irregular, jump-like dissipative liquid meniscus motion between points at which it is temporarily pinned.

We show here, by means of quantitative metallographic analysis of partially infiltrated metal matrix composite materials, that the first mechanism can be discounted, pointing in turn to a dominance of the second mechanism.

Alumina preforms of two types, namely particulate or fibrous, were infiltrated with pure copper, pure aluminium, or an alloy of Al-50 at. pct. Sn. Particulate alumina preforms of average diameter 14mm and height 14mm were prepared by pouring in a single step alumina F-320 particles of average particle size 29 μm, acquired from Treibacher Schleifmittel (Germany), into an alumina mould and then sintering for 10 hours at 1500°C. The alumina volume fraction attained in those particulate preforms was about 0.42, as

* Corresponding author.
E-mail address: andreas.mortensen@epfl.ch (A. Mortensen).

https://doi.org/10.1016/j.scriptamat.2021.114223

determined by comparing the density of the preforms calculated from their weight and dimensions to the density of pore-free alumina (3.99 $g \cdot cm^{-3}$).

Fibrous alumina preforms were prepared from chopped Saffil™ short alumina fibres (produced by ICI in Runcorn, UK), cut from uniaxially pressed silica-bonded fibre disks in which the fibres are arranged in planar random orientation. Samples were cut such that fibres are oriented within a plane perpendicular to the axis of cylindrical preforms having the same dimensions as the particulate preforms.

Infiltration was performed either (i) at 700°C with aluminium (99.99% purity), or (ii) at 1150°C with copper (99.95% purity) or with an alloy of Al-50wt.pct.Sn prepared at EPFL from 99.9% pure tin and 99.99% pure aluminum. This last alloy was selected because its contact angle on alumina is significantly lower than for pure copper or aluminium [13]. The AlSn alloy was prepared in a high-vacuum induction furnace, the chamber of which was initially purged five times with argon. Metals composing the alloy were then melted under argon at 0.8 bar. Once formed, the alloy was poured into a copper mould previously coated with boron nitride.

The gas-driven pressure infiltration chamber that was used to prepare the composites was conceived and designed to dynamically track the metal volume ingress during infiltration of preforms immersed in the molten metal; see Refs [14,15] for a description of the apparatus and method. In essence, the apparatus is a high-temperature analogue to a mercury porosimeter. It comprises a pressure chamber with induction heating and a device that measures dynamically the volume of metal that ingresses into the preform by tracking the movement of a rod attached to a floater resting atop the liquid metal. The metal is driven into the preform against capillary forces that oppose infiltration, by slowly releasing pressurized argon into the evacuated infiltration chamber once the metal is fully molten. The rate of change of the applied gas pressure and the ensuing rate of metal infiltration are sufficiently low for capillary forces to predominate over forces arising from viscous friction or inertial effects. As a result, the melt essentially remains in capillary equilibrium during infiltration. Given the high compliance of pressurized gas, infiltration in this apparatus is de facto conducted under pressure control (as opposed to volume control characteristic of similar room-temperature infiltration experiments conducted in soil science or in studying oil extraction).

Partially saturated samples of this work were prepared by ceasing to increase the gas pressure at a value below the range required for full infiltration, ending the pressure cycle with a hold sufficiently long for the measured rate of metal ingress to have fallen near zero before solidification of the composite. This was done to ensure that the solidified metal geometry be governed chiefly by capillary forces. The solidified, cold, partially infiltrated composite sample was then retrieved, and the remaining pores within it were infiltrated with a reticulating polymeric resin. This was achieved by drilling a small hole into the partially infiltrated composite and then flowing a pressurized epoxy-based resin typically used in metallographic sample preparation (EpoFix, Struers Inc., Cleveland, USA) into the hole in order to fully infiltrate the remaining pores within the composite sample. Samples were then cut and polished following standard procedures for metallographic examination (SiC paper down to 1200 Grit then 6 μm, 3 μm and 1 μm diamond paste with hard cloth, followed by 1µm diamond paste with soft cloth). Unetched microstructures were then observed by scanning electron microscopy in backscattered electron mode (to reinforce phase contrast) using a Zeiss® Merlin SEM (Carl Zeiss, Germany). Local elemental compositions were measured by Energy-Dispersive X-ray spectroscopy (EDX) analysis using an Oxford Instrument apparatus mounted in the SEM with a voltage of 10keV and a probe current of 700 pA. The software ETAS® INCA v.7.0 was used to quantify EDX results. Metallographic characterization gave no signs of the formation of an interfacial reaction phase within the composites of this work.

Microscopic images containing on the order of ten or more reinforcing elements (fibres or particles) along their shorter edge were collected from different parts of each sample in regions containing a homogeneous distribution of the metal phase. From 4 to 10 images were taken of each sample, at up to three magnifications. Only images with metal saturation values that were within 5% of densitometry estimates were used, leading in the end to plot data from 2 to 6 images for each reported composite and saturation.

An image analysis program was developed using available tools within the licensed LabView™ software to quantify the different interfaces present in each image. To this end, the following protocol was applied in turn to each of the three phases present: (i) thresholding each phase so as to distinguish it from the remainder of the microstructure, followed by (ii) quantification of the perimeter of each thresholded phase. It was found by trial and error that no treatment was needed to smooth the phase surfaces (slight smoothing changed the results by less than 2%). It was also unnecessary to adjust the brightness and contrast because the different phases are clearly distinguished on micrographs. Using a greyscale histogram, the threshold values were determined so that the resin phase was between 0 and 55, the particle phase was between 56 and 150, and the metal phase was between 151 and 255 with 0 for white and 255 for black. Only the micrographs of the materials that had been infiltrated with the AlSn alloy required an additional step because precipitates present within this matrix have a similar grey shade to the alumina particles. To address the issue, a size criterion was established for each micrograph, with entities 50 times smaller than the mean area of the largest particles in the micrograph becoming part of the metal phase. It was found that for each micrograph, this operation produced particle volume fractions that were coincident to those of composites with similar preforms infiltrated with Al or Cu, where phase discrimination by image analysis was free of this complication. Fig. 1 shows an original image from a partially infiltrated particulate preform, along with the various thresholds applied to each of the phases, which are coloured in turn in red.

From those three perimeters measured on each 2D micrograph for each phase present, namely the solid alumina (subscript S), the formerly liquid metal infiltrant (subscript L) and uninfiltrated pore space (subscript V, now replaced with resin), relative interfacial perimeters corresponding to each phase were then defined and calculated as indicated in Fig. 2. In a microstructure where the orientation of interfaces is statistically random, as is the case here, each of the three areal interface perimeter values $I_{i\text{-}j}$ (i,j = S, V or L) is $\pi/4$ times the volumetric surface area of the corresponding interface [16]. Given that the microstructure remains statistically the same into the depth of the figure for both the particulate and the fibre composites, ratios of those 2D data are then unbiased samples of the actual 3D volumetric interface surface area ratios within the partially infiltrated composites.

$$I_{S-L} = \frac{P_S + P_L - P_V}{2} \tag{2}$$

$$I_{S-V} = \frac{P_S + P_V - P_L}{2} \tag{3}$$

$$I_{L-V} = \frac{P_L + P_V - P_S}{2} \tag{4}$$

Fig. 3 shows micrographs taken at different metal saturations for the four composite systems. Fig. 4 reports the final result of this work, namely relative interfacial area measurements versus saturation for each of the four systems. Two main conclusions emerge from the data. First, there is for the particulate preforms a nearly

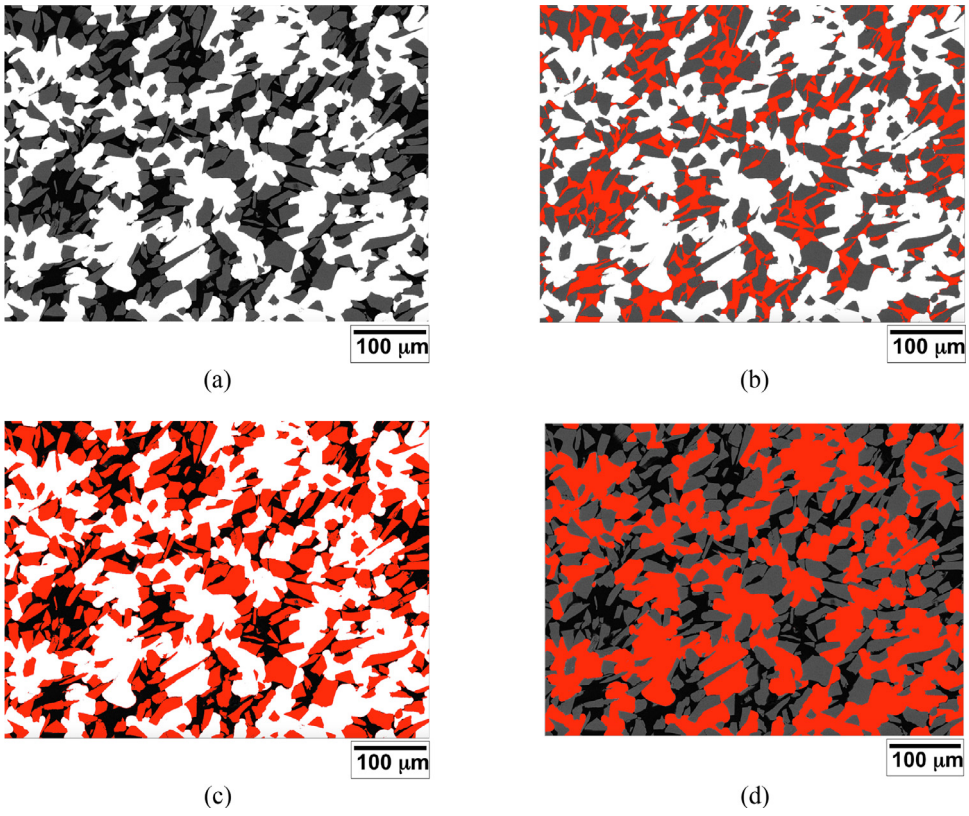

Fig. 1. Phase thresholding in a partially saturated composite of F-320 alumina particles infiltrated with copper: (a) Original image; (b-d) thresholded images showing in red the resin phase (b), particle phase (c) and metal phase (d).

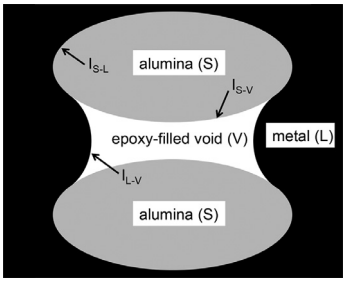

Fig. 2.. Interface perimeter determination from measured phase perimeters (P: perimeter; subscripts S: solid, L: liquid and V: void).

one-to-one correlation between the fraction alumina surface covered with metal and the fraction pore space that is infiltrated. Secondly, the measured liquid/vapour interface area within the composite remains comparatively negligible in equilibrated structures of all stages of the infiltration process across all four composites of this work.

Both observations agree with similar data for the infiltration of samples of soil (see Figs. 7 and 8 of [17]) or of packed spheres (see Fig. 21 of [9]). They also agree with predictions of a recent model for capillarity-dominated infiltration of porous structures containing pinning points (see Fig. 6 of [18]).

The second observation, namely that within the preform the liquid metal/void, i.e., meniscus surface area remains small throughout the infiltration process, differs on the other hand from measurements produced via indirect methods (NMR or tracer tracking) of the water and oil meniscus areas in the infiltration of a fused silica aerolith [19] or of samples of soil or sand [20]. Those studies report liquid meniscus areas that can be well above 10% of the solid phase surface area. The discrepancy may have to do with differences in path or geometry of the samples, or it may result from the existence, within samples of those investigations, of thin films of the liquid whose surface area was evaluated while such films were covering the dry solid phase surface.

The picture that emerges from the present characterization of partially saturated, locally equilibrated, microstructures is thus that the progression of infiltration in metal composite fabrication occurs by the sudden filling of larger pore volumes delineated by several reinforcement elements and separated by constrictions bridged by narrow metal meniscuses. A process of metal infiltration dominated by such jumps (called “Haines jumps” [9, 22]) then explains why liquid meniscus areas measured here are negligibly small while there can still be significant dissipation of irreversible energy in the infiltration process, Fig. 4: pinning of the metal between jumps occurs at narrower constrictions within the preform. The dominance, in initial phases of infiltration, of percolation effects, the importance of which in the context of composite infiltration processing was demonstrated in Ref. [21], further reduces the area of liquid meniscuses in the equilibrated partly infiltrated preform because percolation effects drive infiltration to progress in larger jumps that fill at once several neighbouring pore volumes.

Data of this work are, thus, consistent with a process of infiltration that progresses by intermittent, pinning/depinning jumps. If constriction-separated individual pore volumes are of roughly equal size, as is the case for particulate preforms, then the relation between metal saturation and liquid/solid interface area will be close to linear, while if the pore space is more irregularly sized, as seen for fibrous preforms (Fig. 3), then that curve will deviate from a straight line (and be concave upwards, larger pores being filled first by a poorly wetting infiltrant). A pinning/depinning intermittent jump-dominated progression of infiltration thus also explains the shape of curves in Fig. 4.

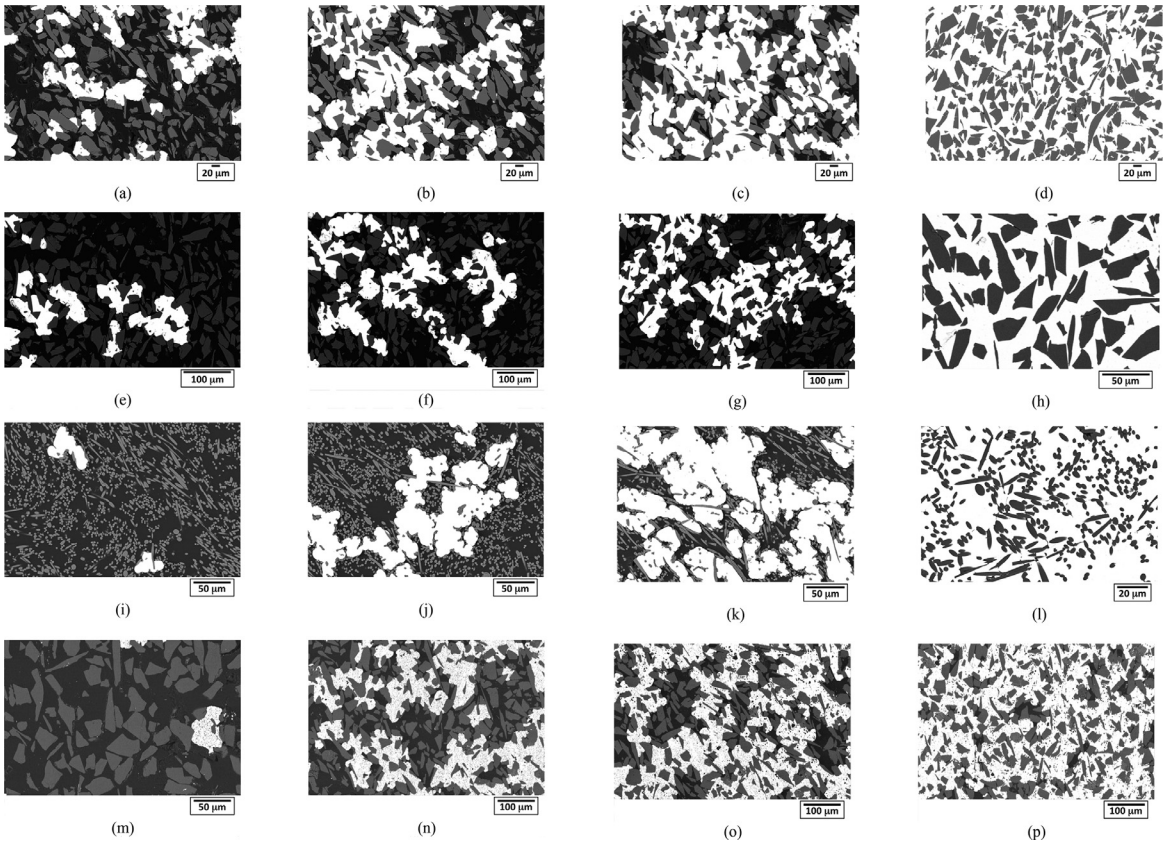

Fig. 3. Metallographic cuts of composites at variable saturation (S): F-320 alumina particles infiltrated with copper at (a) S=0.23, (b) S=0.48, (c) S=0.74 and (d) S=1.00; F-320 alumina particles infiltrated with Al at (e) S=0.10, (f) S=0.17; (g) S=0.26 and (h) S=1.00; Saffil™ preforms infiltrated with copper at (i) S=0.08, (j) S=0.28, (k) S=0.69 and (l) S=1.00; F-320 alumina particles infiltrated with Al-50wt.pct.Sn at (m) S=0.05, (n) S=0.59, (o) S=0.73 and (p) S=0.91.

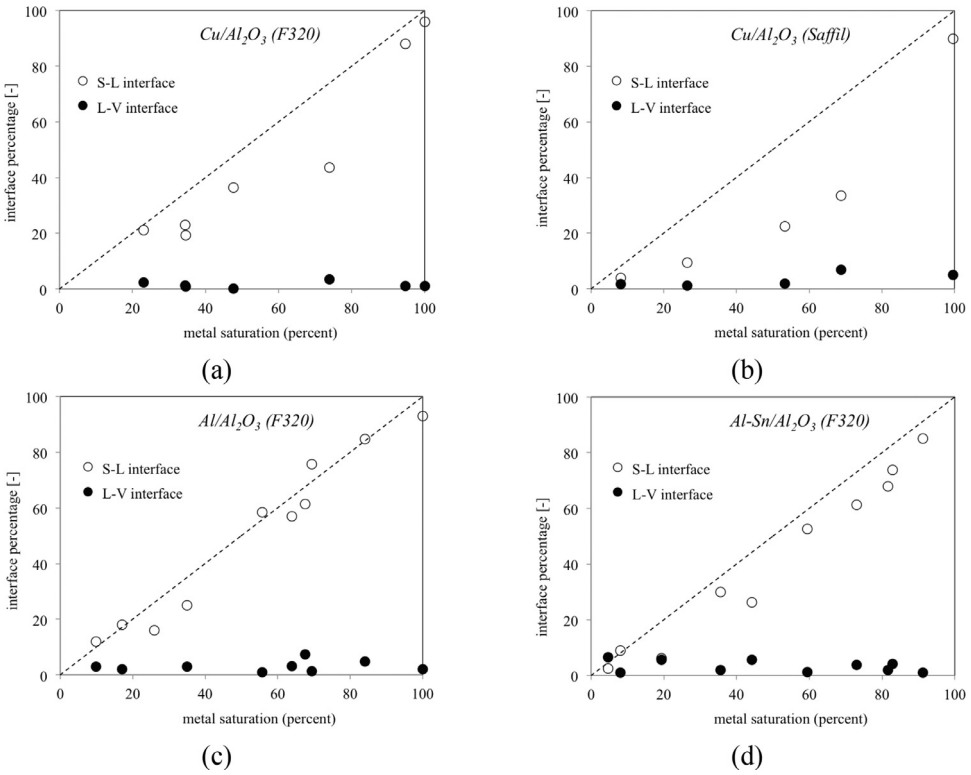

Fig. 4. Ratio of the metal/preform interface and of the metal/void, i.e., meniscus volumetric surface area relative to the preform volumetric surface area, given by $I_{S\text{-}L}/(I_{S\text{-}L} + I_{S\text{-}V})$ and $I_{L\text{-}V}/(I_{S\text{-}L} + I_{S\text{-}V})$ respectively, within the four composites of this work versus the infiltrating metal saturation. The ratio corresponding to the preform/void (solid/void, S-V) surface area is the complement to the sum of the two ratios plotted above.

In conclusion, the present experiments provide experimental confirmation of a mechanism whereby irreversible energy losses that can accompany the infiltration of ceramic preforms with liquid metal are not caused by the temporary creation of significant liquid metal surface area at intermediate phases of the infiltration process. Rather, in the equilibrated partly saturated preform, the liquid metal meniscus surface area remains negligibly small compared to other interfacial areas. Data presented here point to an infiltration process in which irreversible energy is dissipated during sudden ("Haines") jumps, consistent with the simple, pinning-depinning dominated, model of pressure infiltration presented in Ref. [18].

Declaration of Competing Interest

The authors declare the following financial interests/personal relationships which may be considered as potential competing interests.

Acknowledgements

This work was chiefly sponsored by the Swiss National Science Foundation (FNS), Project No. 200021 149899. The authors are grateful to Mr. Willy Dufour of EPFL for his guidance in writing the image analysis code of this work. The authors thank Dr. A. Léger for his assistance in the preparation of the Al-50 at. pct. Sn alloy, and Dr. Ludger Weber, formerly of EPFL now at Tag-Heuer, Switzerland, together with George Varnavides and Prof. W.Craig Carter of MIT for stimulating discussions and helpful suggestions over the course of this work. J.M. Molina-Jordá acknowledges funding from the Spanish "Agencia Estatal de Investigación" (AEI) and the European Union (FEDER funds) through grant MAT2016-77742-C2-2-P.

References

[1] K.K. Chawla, Composite Materials: Science and Engineering, Springer Verlag, New York, 2012 third ed..
[2] R.S. Parnas, Liquid Composite Molding, Carl Hanser Verlag GmbH & Company KG, 2014.
[3] V.J. Michaud, A. Mortensen, Compos. Part A-Appl. S. 32 (2001) 981–996.
[4] V.J. Michaud, Transp. Porous Med. 115 (2016) 581–601.
[5] A. Mortensen, in: Comprehensive Composite Materials, Oxford, Pergamon, 2000, pp. 521–524.
[6] K.M. Sree Manu, L. Ajay Raag, T.P.D. Rajan, M. Gupta, B.C. Pai, Metall. Mater. Trans. B 47 (2016) 2799–2819.
[7] W.B. Hillig, Am. Ceram. Soc. Bull. 73 (1994) 56–62.
[8] J. Bear, Dynamics of Fluids in Porous Media, American Elsevier Pub, New York, 1972.
[9] N.R. Morrow, Ind. Eng. Chem. 62 (1970) 32–56.
[10] F.A.L. Dullien, Porous Media : Fluid Transport and Pore Structure, Academic Press, San Diego, 1992.
[11] J.A. Hunt, R. Ewing, B. Ghanbarian, Percolation Theory for Flow in Porous Media, Springer Verlag, 2014 third ed..
[12] M. Sahimi, Flow and Transport in Porous Media and Fractured Rock: From Classical Methods to Modern Approaches, Wiley-VCH Verlag GmbH&Co, Germany, 2011 second ed..
[13] A. Léger, L. Weber, A. Mortensen, Acta Mater. 91 (2015) 57–69.
[14] M. Bahraini, J.M. Molina, M. Kida, L. Weber, J. Narciso, A. Mortensen, Curr. Opin. Solid St. M. 9 (2005) 196–201.
[15] A. Léger, N.R. Calderon, R. Charvet, W. Dufour, C. Bacciarini, L. Weber, A. Mortensen, J. Mater. Sci. 47 (2012) 8419–8430.
[16] E.E. Underwood, Quantitative Stereology, Addison-Wesley Publishing Company, Reading, MA, 1970 second ed..
[17] S. Seth, N.R. Morrow, SPE Reserv. Eval. Eng. 10 (2007) 338–347.
[18] G. Varnavides, A. Mortensen, W.C. Carter, Acta Mater 210 (2021) 116831.
[19] M. Fleury, J. Colloid Interf. Sci. 509 (2018) 495–501.
[20] S. Peng, M.L. Brusseau, Water Resour. Res. 41 (2005) 1–8.
[21] A. Léger, J.M. Molina-Jordá, L. Weber, A. Mortensen, Mater. Res. Lett. 3 (2014) 7–15.
[22] W.B. Haines, J Agric. Sci. 20 (1930) 97–116.